Hindawi
Advances in Civil Engineering
Volume 2018, Article ID 2690951, 9 pages
https://doi.org/10.1155/2018/2690951

*Research Article*

# Refined Finite Element Analysis of Crack Causes in SRC Arch Rib Bridges considering Multiple Factors

**Mengsheng Yu**,[1] **Nianchun Deng**,[1] **Qifeng Chen**,[2] **and Tianzhi Hao**[2]

[1]*College of Civil Engineering and Architecture, Guangxi University, Nanning 530007, China*
[2]*Guangxi Transportation Research & Consulting Co., Ltd., Nanning 530007, China*

Correspondence should be addressed to Mengsheng Yu; xiaoluo19890316@163.com

Received 26 April 2018; Revised 20 October 2018; Accepted 24 October 2018; Published 15 November 2018

Academic Editor: Stefano de Miranda



The SRC (steel-frame reinforced concrete) arch bridge is an important part of the development of arch bridges. Scholars worldwide have studied it from various aspects because of its stronger stiffness and stability than other types of bridges especially when crossing the canyon. The steel frame is a stress bracket during construction. Concrete becomes the main axial-pressure bearing structure when it fills the inner pipe and the encased frame. This article mainly focuses on the crack problems of SRC arch bridging during the postconstruction operation, local model of the midspan arch rib, and the equivalent relationship between the coefficient of expansion and the temperature of concrete. This study uses a cooling method to simulate the shrinkage process with detailed analysis of three properties including concrete shrinkage, temperature gradients, and concentrated hanger rod force. It is concluded that the SRC arch bridge will have large tensile stress on both inner and outer surfaces of slab and web when the temperature changes, and it is the main cause of cracks. The results agree well with measured data. At last, we come up with some reference suggestions in the design and construction of similar bridges in the future.

## 1. Introduction

Arch bridge construction is one of the most common bridging methods, and there is already much research on it from various aspects [1–5]. From the early stone arch to the reinforced concrete arch to the steel arch and steel-concrete composite arch bridge, the most advanced arch bridge construction technology is in China, where the longest span (445 meters) SRC arch bridge is built [6–9]. With the continuous improvement of construction materials, construction technology, and design concept, more and more long-span arch bridges have been built both in China and other countries. In the past 20 years, seven bridges with spans of more than 300 m have been built [10, 11]. SRC arch bridge design stands out from many arch bridges because of its light weight, high rigidity, strong spanning ability, convenient construction, good structural integrity, etc., and it becomes the first choice for arch bridge spans over 200 m in China's mountainous canyon area.

There have been many successful exemplary projects of steel-frame reinforced concrete (SRC) arch bridges with spans of more than 200 m both in China and other countries and districts [12–14]. In 1942, Spain built the Esla arch bridge with a span of 210 m which was the longest span SRC arch bridge in the world at that time [14, 15]. The Yongjiang bridge, Yongning, was built in 1996 with a span of 312 m, the Wanxian Yangtze River bridge was built in 1997 with a span of 420 m, and the Shanghai–Kunming Beipanjiang Railway bridge was built in 2016 with a span of 445 m. In 2003, Japanese designers even attempted to design a 600 m SRC arch bridge [16, 17]. The original complete plan of the Miller bridge built in 2004 in France is a 602 m SRC arch bridge [18]. At present, most scholars study the construction methods and the process of SRC arch bridges. But the studies lack detailed analysis. In 1992, academician Zheng Jielian published a method that uses the oblique cable to hang arch ribs during construction adopting jack control technology and continuously poured concrete arch rib technology. It

has been widely used in the construction of large-span SRC arch bridges in China because of lower transient and permanent stresses [19]. Xie et al. [20] found that new stress redistribution in arch rib sections caused by shrinkage and creep cannot be ignored through the comparative study of shrinkage and creep theory and the model experimentation. Zhou [21] did shrinkage and creep model experiments to study layered-pour concrete arch ribs. Additionally, Lin et al. [22] summarized the progress of the study on voids in concrete-filled steel tubular structures.

In this paper, we mainly use the ANSYS software to simulate the stress state of the SRC arch ribs in the course of construction and analyze the causes of arch rib cracks from three aspects, which are shrinkage and creep from concrete, the temperature gradients in arch rib cross sections, and rod tension. The calculated results are in agreement with the measured results.

## 2. Concrete Shrinkage Theories of Arch Ribs

Steel-frame reinforced concrete (SRC) arch bridging is one type of steel-concrete composite structure. The bonding surface between steel and concrete is an important feature and needs to be studied deeply. With the passage of time, shrinkage and creep of concrete increase gradually [23]. In this article, for the relevant parameters of concrete shrinkage, refer to Appendix F of "Code for Design of Highway Reinforced Concrete and Prestressed Concrete Bridges and Culverts" which is the Chinese Bridge specification [24]:

$$\varepsilon_{cs}(t,t_s) = \varepsilon_{cso} \cdot \beta_s(t-t_s), \tag{1}$$

$$\varepsilon_{cso} = \varepsilon_s(f_{cm}) \cdot \beta_{RH}, \tag{2}$$

$$\varepsilon_s(f_{cm}) = \left[160 + 10\beta_{sc}\left(9 - \frac{f_{cm}}{f_{cmo}}\right)\right] \cdot 10^{-6}, \tag{3}$$

$$\beta_{RH} = 1.55\left[1 - \left(\frac{RH}{RH_0}\right)^3\right], \tag{4}$$

$$\beta_s(t-t_s) = \left[\frac{(t-t_s)/t_1}{350(h/h_0)^2 + (t-t_s)/t_1}\right]^{0.5}, \tag{5}$$

where $t$ is the age of concrete when calculated (days, d); $t_s$ is the shrinkage at the beginning of the concrete age (days, d) and here can be assumed to be 3 d–7 d; $\varepsilon_{cs}(t,t_s)$ is the shrinkage strain when the calculated concrete age is "$t$" while the initial age is "$t_s$"; $\varepsilon_{cso}$ is the nominal contraction coefficient; $\beta_s$ is the coefficient of contraction with time; $f_{cm}$ is the concrete average cubic compressive strength (MPa) with strength grade C20–C50 at the age of 28 d, $f_{cm} = 0.8f_{cu,k} + 8$ MPa; where $f_{cu,k}$ is the concrete cubic compressive strength standard value (MPa) with 95% guarantee rate at the age of 28 d; and $\beta_{RH}$ is the coefficient of annual average relative humidity. In formula (4), it applies to 40% < RH < 90%; RH is the annual average relative humidity (%); $\beta_{sc}$ is a coefficient describing the type of cement, for Portland cement and quick hardening cement, $\beta_{sc} = 5.0$; $h$ is the component theory thickness (mm), $h = 2A/\mu$, $A$ is the cross-sectional area of the member and $\mu$ is the contact length with the atmosphere; $RH_0 = 100\%$; $h = 100$ mm; $t_1 = 1$ d; $f_{cmo} = 10$ MPa.

A cooling method is used to simulate the shrinkage and the creep of concrete in finite element model analysis. The equivalent temperature drop value "$T(t)$" at the time of "$t$" can be expressed as

$$T(t) = \frac{\varepsilon_{cs}(t,t_s)}{\alpha_c}. \tag{6}$$

where the coefficient of the linear expansion of $\alpha_c$ is $1 \times 10^{-5}$.

## 3. Analysis of Arch Ribs in SRC Arch Bridges

The object of this paper is a long-span SRC arch bridge constructed many years ago. The elevation diagram is shown in Figure 1. The crack propagation of the number one (#1) arch rib is shown in Figures 2 and 3. A photo of the bridge under study is shown in Figure 4. The crack distribution of the number two (#2) arch rib is similar to that of #1 arch rib, and thus no list of it is given. It can be seen from the diagrams that the cracks mainly appear on the region near the top arch rib, especially on both inner and outer surfaces of the slab and web of the arch rib. And the phenomenon is very common.

To analyze the cause of the formation of long longitudinal cracks on arch ribs, a numerical simulation is carried out where mainly shrinkage and temperature gradients are taken into consideration. Through the investigation of the arch rib crack forming time, it is found that the longitudinal crack in arch ribs is partially formed during the curing period of the main arch rib. At this stage, the arch rib is only affected by its own weight due to gravity, while the axial force and bending moment produced by this self-weight is not strong enough to lead to the longitudinal cracks in the arch ribs. Therefore, the cause of cracks can be narrowed to concrete shrinkage and temperature gradient and others.

*3.1. Refinement Analysis Model of Arch Ribs in SRC Arch Bridges in China.* This article chose a midspan of main arch ribs to make refined finite element analysis and constructive analysis according to the investigation of arch rib cracking in SRC arch bridges. The length of the main arch rib section is 8.92 m, the height is 5 m, the width is 3 m, the thickness of the web is 32 cm, and the thickness of the bottom slab is 0.36 m. The model takes the steel skeleton in the section into account, using the equivalent elastic modulus method to generate the same parameter steel pipe with a diameter of 402 mm and a thickness of 29.2 mm. The SOLID45 element is used to simulate concrete about 33,328 variable units in the model. The BEAM188 element is used to simulate the rigid steel frame about 2,000 variable units. Gravity is applied in the negative direction at a magnitude of 9.8 kN along the $Y$ axis. Considering that deformation of a steel skeleton in concrete is so small that almost no distortion occurs during shrinkage, we constrained the eight corners of the

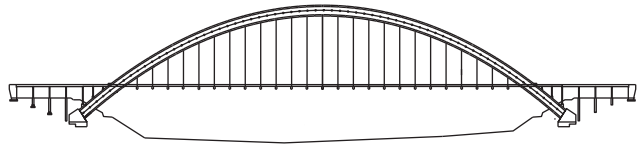

Figure 1: SRC arch bridge elevation.

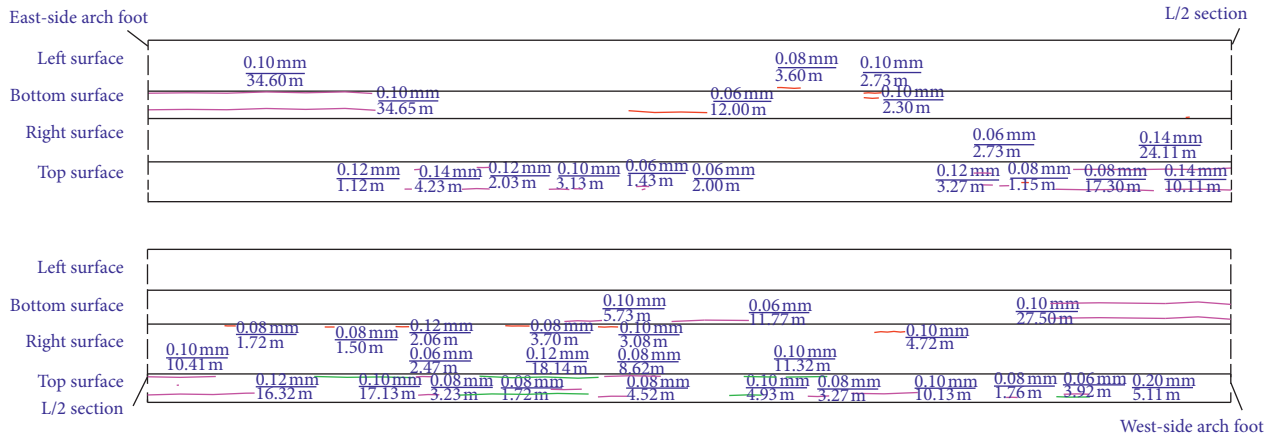


Figure 2: Crack distribution outside #1 arch rib.

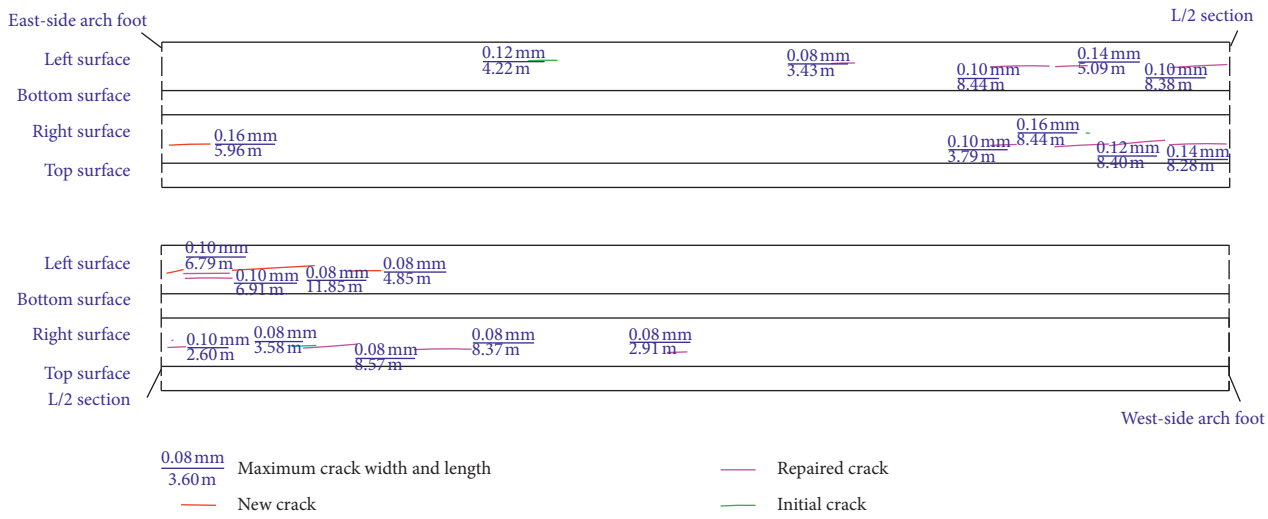


Figure 3: Crack distribution inside #1 arch rib. Note that the crack length and width are not marked when the length is less than 1 m.


(a) (b)

Figure 4: Photos of the bridge under study.

steel skeleton in the model. The finite element model and boundary conditions are shown in Figures 5 and 6. In the model, the relative slip between steel frame and concrete is not considered as small deformation. We think that it is in the stage of elastic stress during the whole work. The important mechanical parameters used in the analyses are shown in Table 1.

*3.2. Effect of Concrete Shrinkage in Arch Ribs.* For the SRC arch bridge and other bridge types, new distribution of the internal stresses due to the shrinkage of concrete on the joining surface between concrete and steel can be simulated by the finite element method. From the calculation of the cross section of the arch rib, the shrinkage strain of the structure can be obtained at each age, as shown in Table 2.

*3.2.1. Stress Distribution of Shrinkage.* Through the model calculations, we finely get the stress distribution at the bottom of the slab and the web of the arch rib after 30 days of shrinkage, 180 days of shrinkage, and 3600 days of shrinkage, which are typical in different periods of time. The results are shown in Figures 7–9.

*3.2.2. Effects of Concrete Shrinkage on Arch Ribs*

(1) The results show that tensile stress on the outer surface of the bottom slab is larger at the end of the arch ribs because of concrete shrinkage, and the maximum tensile stress reaches 1.595 MPa at the age of 30 days, 2.554 MPa after 180 days, and then 2.898 MPa after 3600 days. The reason is that the steel frame imposes strong constraints on the concrete.

(2) The inner surface of the arch rib bottom slab is in a minimal pressure or a tensile stress state.

(3) The inner surface of the arch rib web is pulled, and the maximum tensile stress reaches 1.851 MPa at the age of 30 days, 2.964 MPa after 180 days, and then 3.363 MPa after 3600 days.

(4) The outer surface of the arch rib web is pulled, too. The maximum tensile stress of the arch rib web reaches 0.562 MPa at the age of 30 days, 0.901 MPa after 180 days, and then 1.022 MPa after 3600 days.

## 4. Analysis of the Influence of Temperature Gradients and Suspension Concentration on Arch Rib Cracking

The bridge is located in Nanning, Guangxi Province. The lowest monthly average temperature is 12.8°C in January, and the highest one is 28.2°C in July and August according to the statistics of Nanning Meteorological Bureau.

In the FEA model shown in Figures 5 and 6, we chose two temperature gradients, one at 10 and the other at −10°C. The rib element is divided into three layers from outside to inside, and each layer is subjected to a gradually increased or decreased temperature. The model of the cooling gradient is shown in Figure 10.

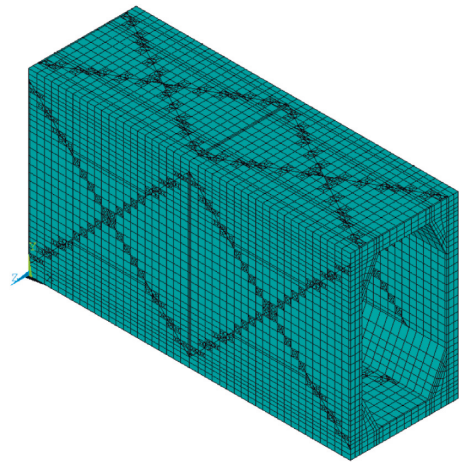

Figure 5: FEM of midspan arch rib concrete element.

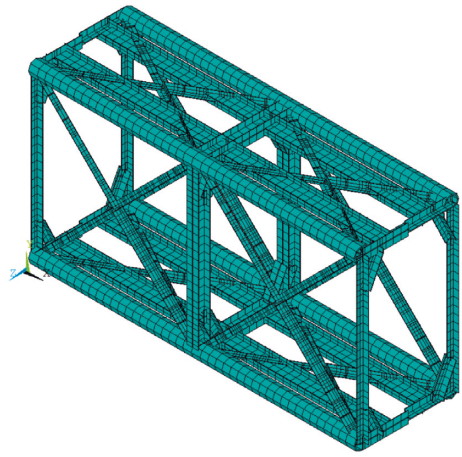

Figure 6: FEM of midspan arch rib—stiff skeleton element.

*4.1. Effects of the Temperature Gradient on Arch Rib Cracking*

*4.1.1. The Results of Cooling Gradient.* When the gradient temperature is −10°C, the inner surface of the rib is compressed, while the outer surface is under tension. The transverse tensile stress on the outer surface of the web is from 2.523 MPa to 3.214 MPa. The temperature stress distribution is shown in Figure 11.

*4.1.2. The Results of the Rising Gradient.* When the gradient temperature is 10°C, the inner surface of the rib is under tension, while the outer surface is compressed. The maximum transverse tensile stress on the inner surface of the web is 2.723 MPa. The temperature stress distribution is shown in Figure 12.

*4.2. Effect of Suspension Concentration on Arch Rib Cracking.* The boom is anchored to the ribs through the boom support block. The detailed analysis of this region shows that the tensile stress of the bottom plate and web plate near the anchor point of the suspender will appear in the action of the 1300 kN suspender force. The maximum transverse tensile

Table 1: Mechanical parameters used in the analyses.

| Parameter | Elastic modulus (MPa) | Poisson ratio | Density (kg/m$^3$) | Coefficient of linear expansion (1/°C) |
|---|---|---|---|---|
| Steel | $2.06e + 5$ | 0.3 | $7.8e + 3$ | $1.2e - 5$ |
| Concrete | $3.45e + 4$ | 0.2 | $2.6e + 3$ | $1.0e - 5$ |

Table 2: Stress in Arch rib of different concrete ages.

| Time (days) | 30 | 60 | 90 | 180 | 360 | 720 | 3600 |
|---|---|---|---|---|---|---|---|
| Strain ($\mu\varepsilon$) | 153 | 197 | 218 | 245 | 261 | 270 | 278 |
| Temperature, $T$ | 15.3 | 19.7 | 21.8 | 24.5 | 26.1 | 26.9 | 27.8 |

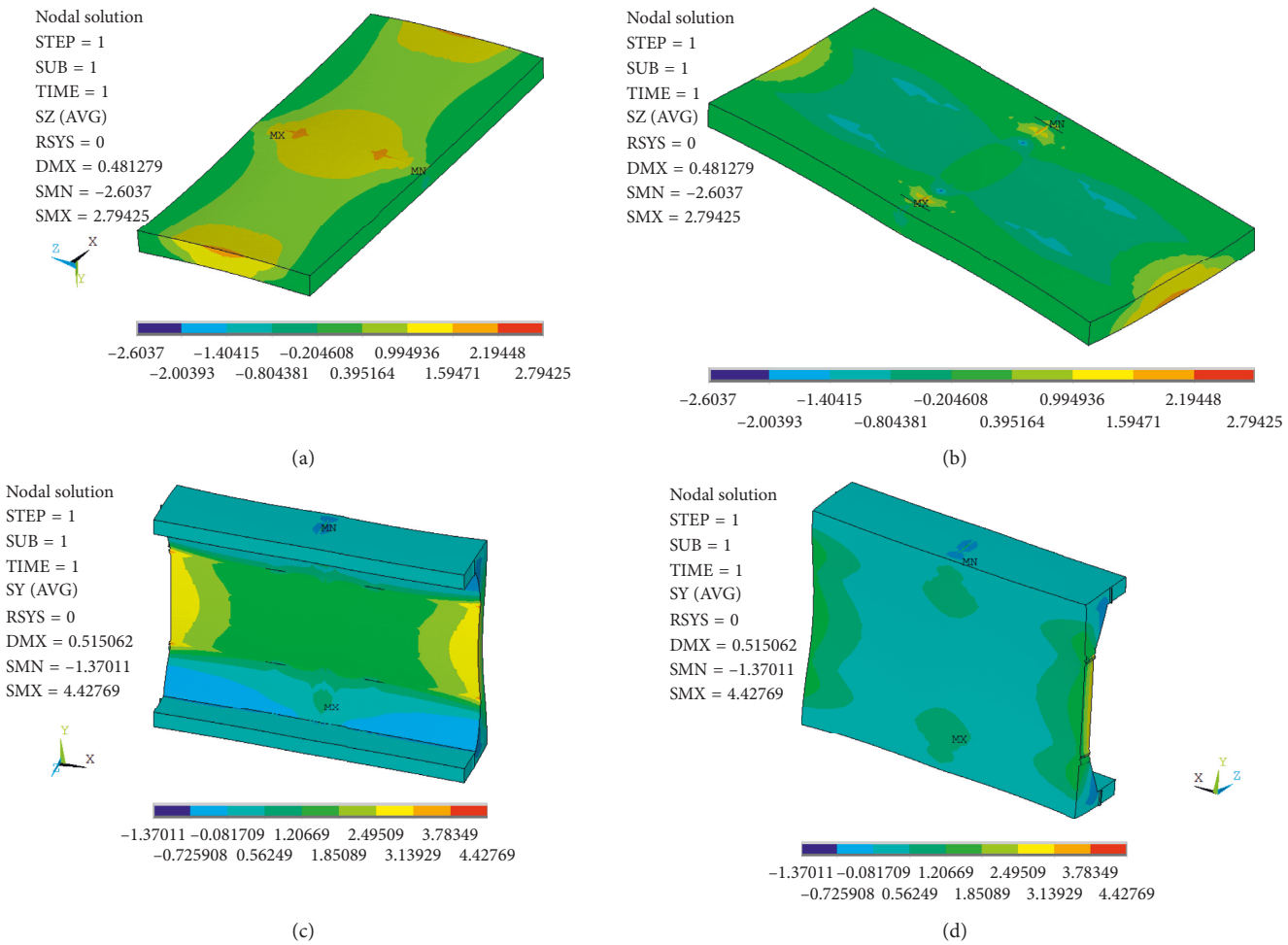


Figure 7: Stress distribution in bottom of the slab and web of the arch rib after 30 days' shrinkage (unit: MPa). Normal stress distribution in $Z$-direction on (a) the inner surface of the bottom slab and (b) the outer surface of the bottom slab. Normal stress distribution in the $Y$-direction on (c) the inner surface of the web and (d) the outer surface of the web.

stress of the bottom plate is 2.241 MPa, and the maximum lateral tensile stress of the web is 1.458 MPa, as are shown in Figures 13 and 14.

## 5. Conclusion

In this paper, finite element software is used to simulate the stress of the vault arch rib section. After analyzing the three properties of concrete shrinkage, temperature gradients, and concentration of the suspension, we come to the following conclusions:

(1) Influenced by concrete shrinkage, the outer surface of both top and bottom arch ribs and the inner surface of the web will be under larger tensile stress. The tensile strength of concrete C50 is 2.65 MPa

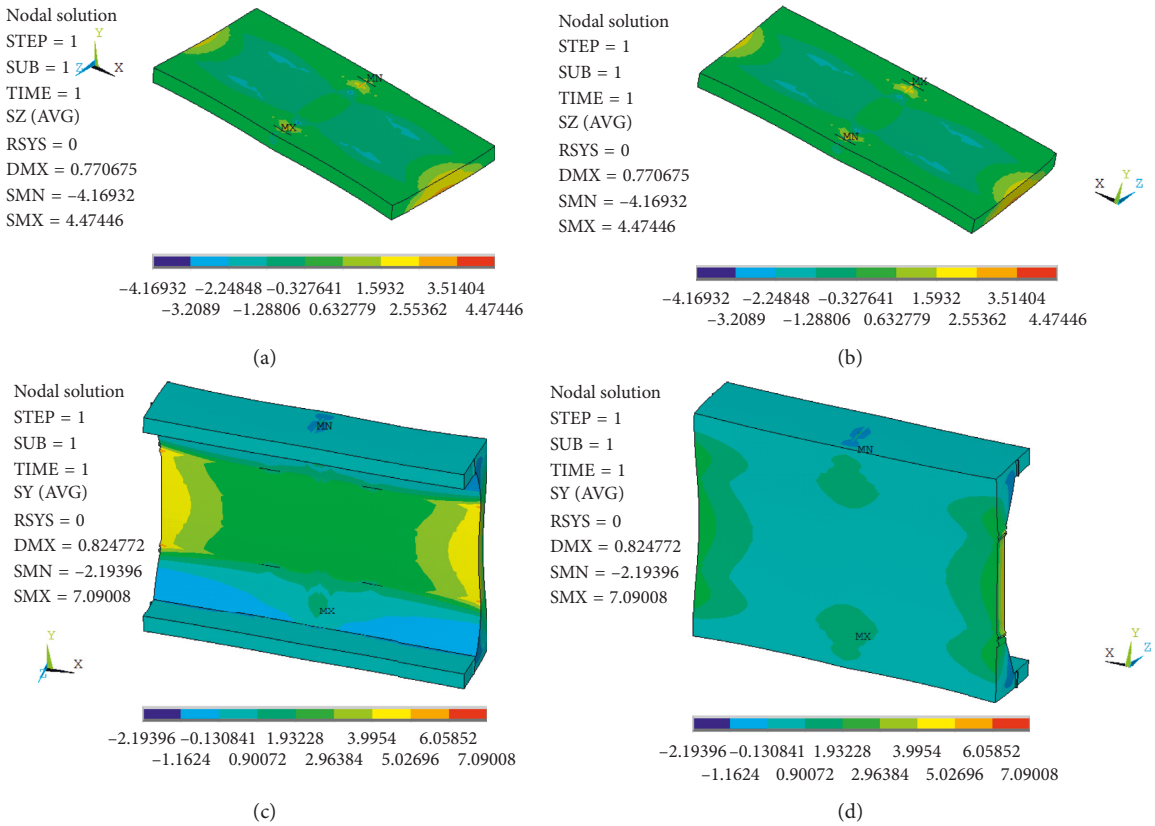


Figure 8: Stress distribution in bottom of the slab and web of the arch rib after 180 days' shrinkage (unit: MPa). Normal stress distribution in $Z$-direction on (a) the inner surface of the bottom slab and (b) the outer surface of the bottom slab. Normal stress distribution in the $Y$-direction on (c) the inner surface of the web and (d) the outer surface of the web.

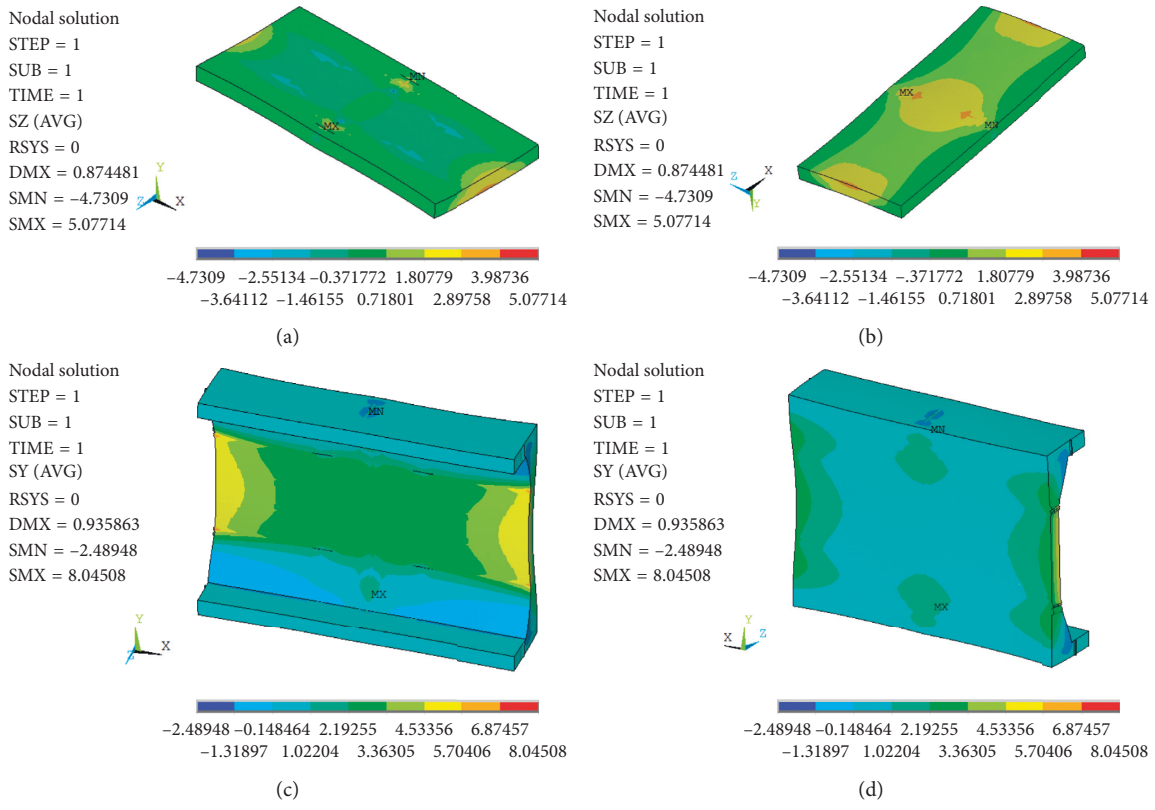


Figure 9: Stress distribution in bottom of the slab and web of the arch rib after 3600 days' shrinkage (unit: MPa). Normal stress distribution in $Z$-direction on (a) the inner surface of the bottom slab and (b) the outer surface of the bottom slab. Normal stress distribution in the $Y$-direction on (c) the inner surface of the web and (d) the outer surface of the web.

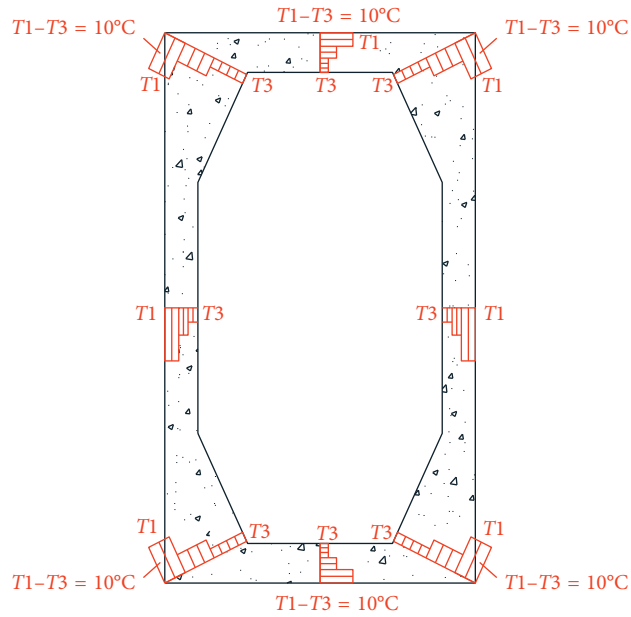


Figure 10: Temperature gradient distribution in the arch rib model.

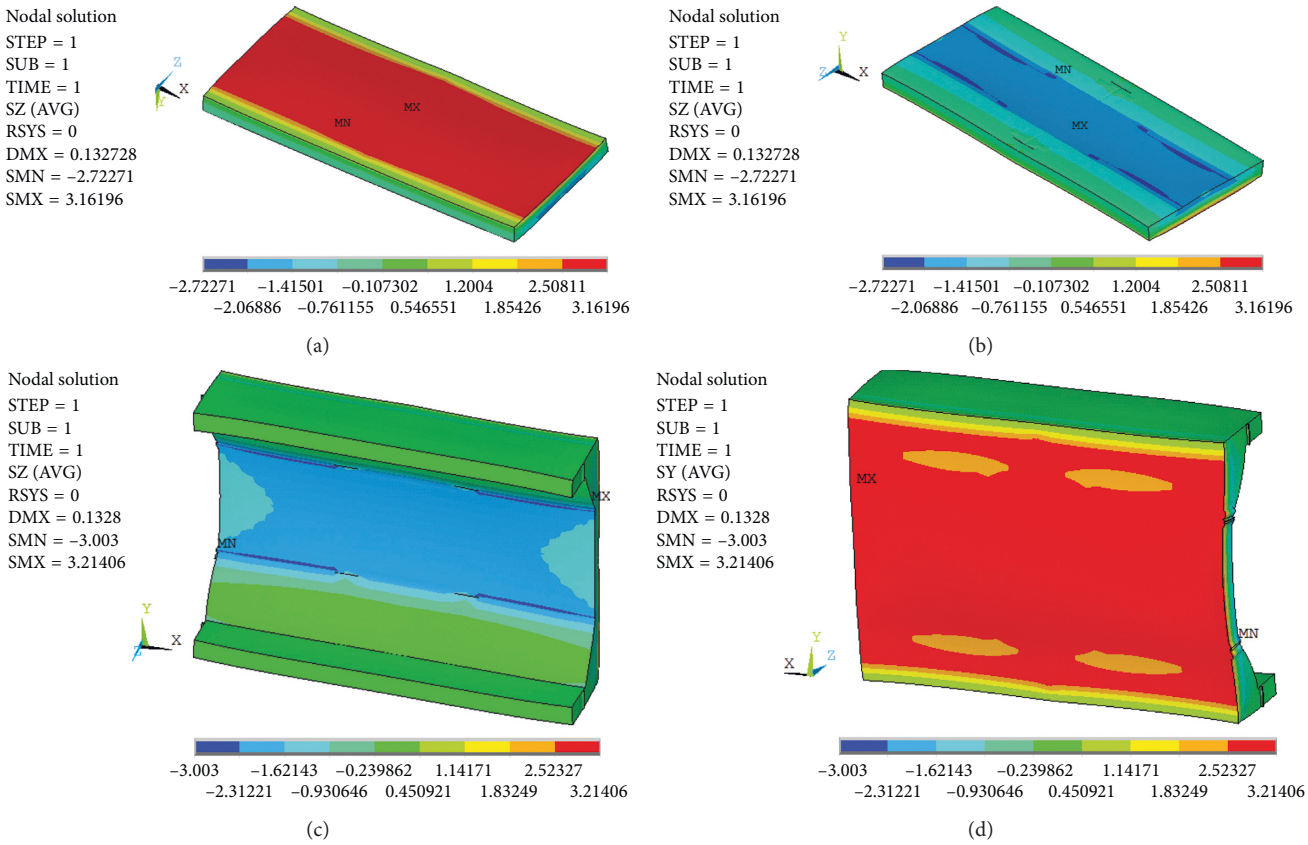


Figure 11: Stress distribution in bottom of the slab and web of the Arch rib when the temperature gradient drops 10°C. Normal stress distribution on (a) the inner surface of the bottom slab; (b) the outer surface of the bottom slab; (c) the inner surface of the web; (d) the outer surface of the web.

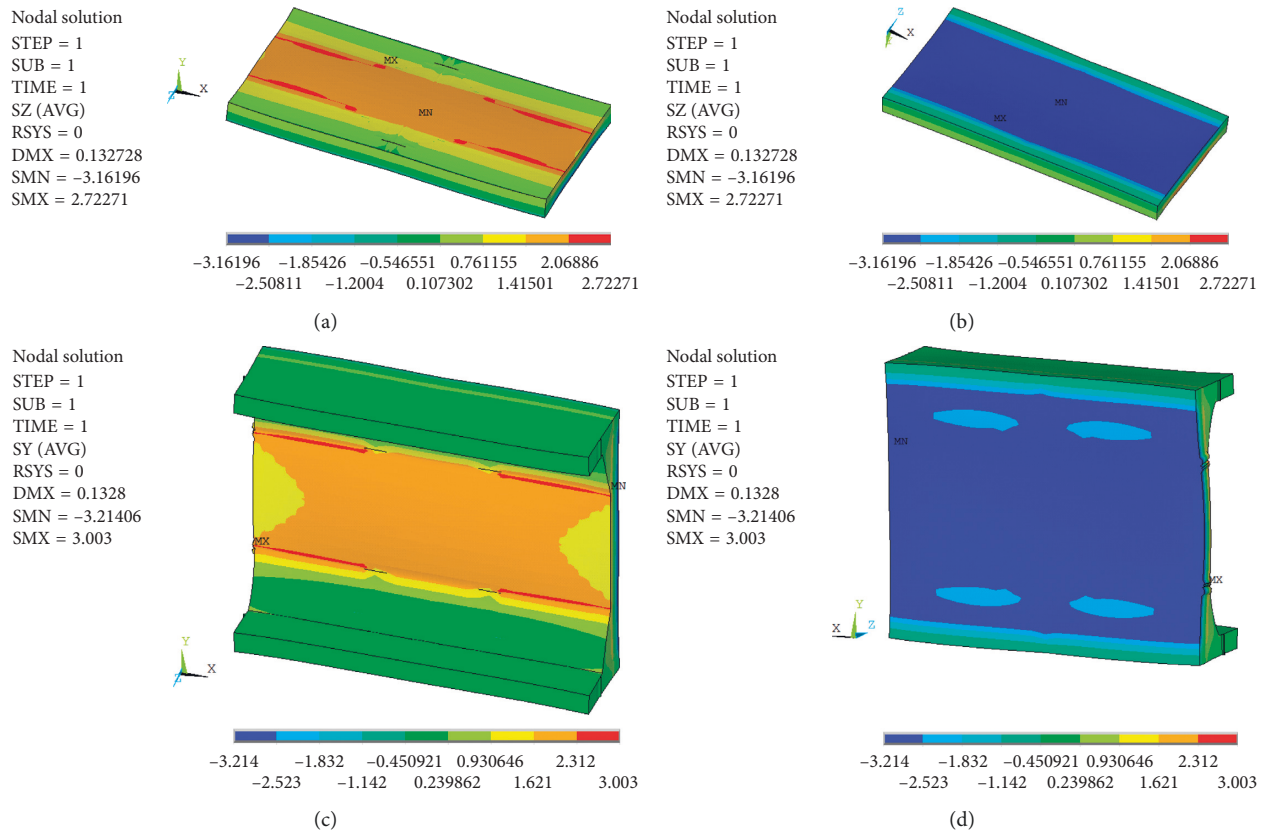


Figure 12: Stress distribution in bottom of the slab and web of the arch rib when the temperature gradient rises 10°C. Normal stress distribution on (a) the inner surface of the bottom slab; (b) the outer surface of the bottom slab; (c) the inner surface of the web; (d) the outer surface of the web.

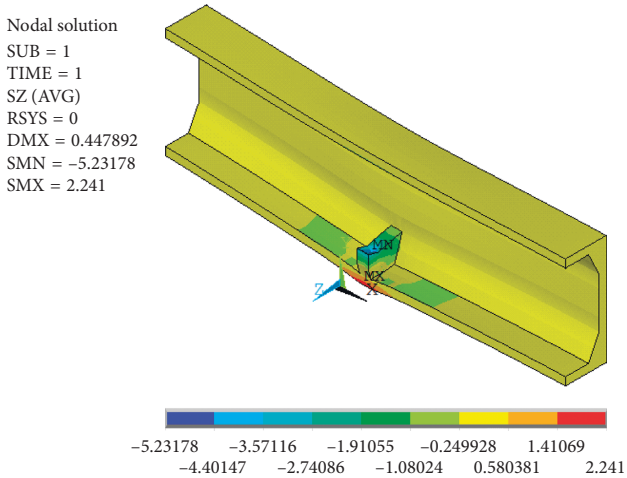


Figure 13: Cross stress distribution in the bottom slab of the arch rib.

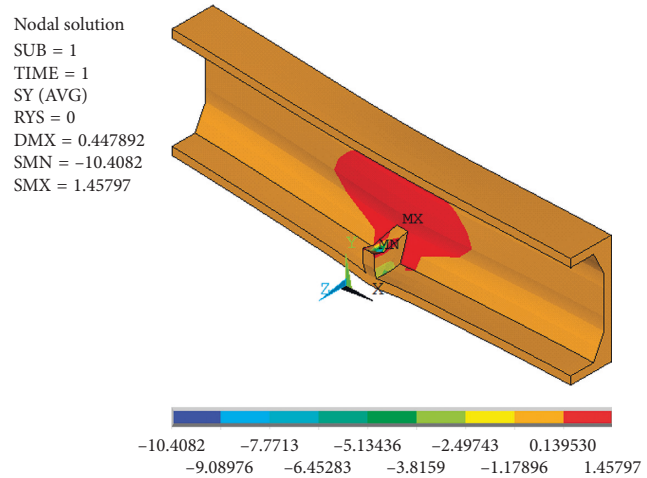


Figure 14: Cross stress distribution in the web of the arch rib.

according to the Chinese bridge standard. But, the tensile stress value of the web and the bottom plate is more than C50 concrete's design value which is an important factor in crack initiation. The results of finite element analysis are consistent with the results of visual inspection. The longitudinal crack on the outer surface of #1 arch rib is more common in the vault and arch bottom, while the longitudinal crack on the inner surface is more common in the web.

(2) Due to the rapid change in atmospheric temperature and the temperature change in the arch rib being slow, the temperature gradient will exist along the thickness direction of arch ribs. Assuming that the temperature gradient between inner and outer ribs is

10°C, we confirm that the inner surface of the arch rib will be under pressure, while the outer surface of the upper side will be under tension when the air temperature is lowered. Thus, the tensile strength of the outside surface is over the design value. When the air temperature rises, the outer surface of the arch rib will be under pressure, while the internal surface will be under tension, and the tensile stress of the inner surface is over the design value. What is more, the process of temperature change will further aggravate crack development in arch ribs.

(3) The design tensile force of the suspender is 1300 kN and the tensile stress of the bottom plate and the web of the arch rib will increase during the operating process. This phenomenon will be aggravated with the repeated action of the vehicle load in the post-bridge operation process. By the way, longitudinal cracks in reinforced concrete arch bridges arch rib are allowed when the width is less than the allowable value. But, we must pay attention to this problem because of its effects on durability of bridges.

## Data Availability

The testing and analysis data used to support the findings of this study are included within the article.

## Conflicts of Interest

We declare that there are no conflicts of interest regarding the publication of this paper.

## Acknowledgments

This study was partly sponsored by the following fund programs: (1) Guangxi Science and Technology Program (code: 2016AC06007); (2) Nanning Scientific Research and Technology Development Plan (Code: 20160319); (3) Guangxi Key Sci-Tech Problems Tackling Program (GKG 1598009-1); (4) Guangxi Natural Science Fund Research Program (2015GXNSFBA139229); (5) Project (KY2015YB006) supported by the Guangxi Higher Educational Science Research Program.

## References

[1] R. W. Furlong, "Design of steel-encased concrete beam-columns," *Journal of Structural Division*, vol. 94, p. 15, 1968.

[2] S. H. Ju, "Statistical analyses of effective lengths in steel arch bridges," *Computers and Structures*, vol. 81, no. 14, pp. 1487–1497, 2003.

[3] A. S. Nazmy, "Stability and load-carrying capacity of three-dimensional long-span steel arch bridges," *Computers and Structures*, vol. 65, no. 6, pp. 857–868, 1997.

[4] S. H. Kwon, T. H. Kim, Y. Y. Kim, and J. K. Kim, "Long-term behavior of square concrete-filled steel tubular columns under axial service loads," *Magazine of Concrete Research*, vol. 59, no. 1, pp. 53–68, 2007.

[5] Y. Wang, Y. Geng, G. Ranzi, and S. Zhang, "Time-dependent behavior of expansive concrete-filled steel tubular columns," *Journal of Constructional Steel Research*, vol. 67, no. 3, pp. 471–483, 2011.

[6] J. L. Zheng, "New development tendency of large-span reinforced concrete arch bridges in China," *Journal of Chongqing Jiaotong University*, vol. 1, p. 4, 2016.

[7] J. Zheng, "Development and technical progress of arch bridge in China," in *Forum on Highway Science and Technology Innovation in Hubei Province*, vol. 6, Heritage Hills Society, Hubei, China, 2016.

[8] J. Wei and B. C. Chen, *Application and Research Advancement of Long Span Concrete Arch Bridges Abroad*, World Bridges, vol. 2, pp. 4–8, 2009.

[9] B. C. Chen, J. Su, S. Lin, G. Chen, Y. Zhuang, and H. Tabatabai, "Development and application of concrete arch bridges in China," *Journal of Asian Concrete Federation*, vol. 3, no. 2, pp. 12–19, 2017.

[10] J. Salonga and P. Gauvreau, "Comparative study of the proportions, form, and efficiency of concrete arch bridges," *Journal of Bridge Engineering*, vol. 19, no. 3, 2014.

[11] J. Radić, A. Kindij, and A. Mandić-Ivanković, "History of concrete application in development of concrete and hybrid arch bridges," *Long Arch Bridges*, vol. 11, 2008.

[12] B. C. Chen and Q. W. Huang, "Study on the design of 600 m span concrete arch bridge," *Journal of China and Foreign Highway*, vol. 26, p. 3, 2006.

[13] W. Q. Mao, "Construction design of lifting and erection of long span reinforced concrete arch bridge," *Bridge Construction*, vol. a01, pp. 18–21, 2007.

[14] L. F. Troyano, "Procedures for the construction of large concrete arches," in *Proceedings of the Fourth International Conference on Arch Bridges*, Barcelona, Spain, November 2004.

[15] T. Mori, T. Yamamoto, N. Tamehiro, and J. Niwa, "The state of the art and the future prospects on long-span concrete arch bridges," *Canadian Journal of Sociology*, vol. 39, no. 3, pp. 12–20, 2001.

[16] B. C. Chen, "Research on progress of super long-span concrete arch bridge," in *The Seventeenth National Academic Conference on Bridges*, Institute Baseboce, China Communications Press, Chongqing, China, 2006.

[17] J. Muller, "On design and construction of long span concrete arch bridge," in *Proceedings of the Third International Conference on Arch Bridge*, vol. 10, Paris, France, 2001.

[18] J. B. Zlatko Šavor, "Long span concrete arch bridges of europe," in *Chinese-Croatian Joint Colloquium on Long Arch Bridges*, University of Zagreb, Zagreb, Croatia, 2008.

[19] J. Zheng, "Discussion on technology of suspending and connecting for the RC bridge with an unusual large span," *China Journal of Highway and Transport*, vol. 8, 1999.

[20] X. L. Xie, R. Qin, and W. L. Peng, "Theoretical analysis of creep and shrinkage effects in SRC arch bridge," *Engineering Science*, vol. 5, 2001.

[21] S. Zhou and A. Gu, "Creep-shrinkage model test of concrete box Arch of division layer pouring," *China Journal of Highway and Transport*, vol. 7, 1997.

[22] C. J. Lin, J. L. Zhu, and R. Qin, "Review of concrete confined concrete filled steel tubular arch rib," *Journal of China and Foreign Highway*, vol. 5, 2004.

[23] Z. P. Bažant and L. Panula, "Creep and shrinkage characterizations for analyzing prestressed concrete structures," *PCI Journal*, vol. 25, no. 3, pp. 86–122, 1980.

[24] Standard PsRoCi, *Code for Design of Reinforced Concrete and Prestressed Concrete Bridges and Culverts*, The Ministry of Communications of the People's Republic of China, Beijing, China, 2004.